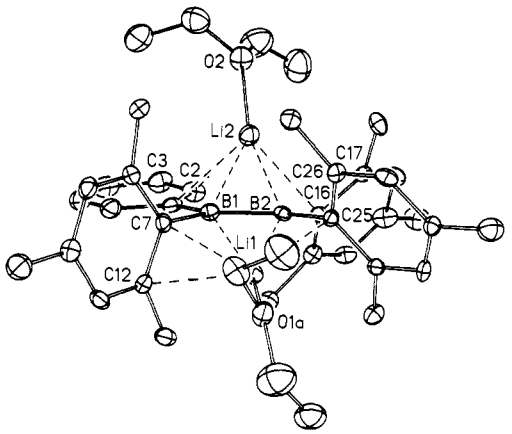

Figure 1. Computer-generated thermal ellipsoid plot of 1. Some important bond distances (angstroms) and angles (degrees) not given in the text or Table I are as follows: Li(1)-O(1a) = 1.962 (15), Li(1)-O(1b) = 1.927 (22), Li(2)-O(2) = 1.918 (15); B(2)-B(1)-C(1) = 124.6 (4), B(2)-B(1)-C(7) = 125.8 (6), B(1)-B(2)-C(16) = 122.2 (6), B(1)-B-(2)-C(25) = 128.8 (6). Interplanar angles between the averaged planes at the following atoms are as follows: B(1) and C(1), 6.3°; B(1) and C(7), 86.8°; B(2) and C(16), 56.8°; B(2) and C(25), 56.6°.

Table I. Selected Bond Distances (Å) and Angles (deg) in 1 and 2

	1	2
B(1)-B(2)	1.636 (11)	1.706 (12)
B(1)-C(1)	1.613 (11)	1.565 (12)
B(1)-C(7)	1.648 (7)	1.579 (11)
B(2)-C(16)	1.642 (10)	1.576 (9)
B(2)-C(25)	1.643 (11)	1.586 (12)
C(1)-B(1)-C(7)	109.5 (5)	115.1 (7)
C(10)-B(2)-C(25)	108.9 (6)	119.8 (6)
angle between B(1) and B(2) planes	7.3	79.1

alkali metal, R = organo group) have been structurally characterized to date. The contrast between 1 and the structures of the dimeric lithium salts of alkyls, aryls, amides, phosphides, or alkoxides further emphasizes the unique structural features observed in 1.[14]

Finally, it is notable that calculations[15] on the parent compound $Li_2B_2H_4$ show that it is planar and thermodynamically very stable and has a B-B distance of 1.613 Å. An alternative configuration, in which the Li^+ ions are disposed above and below the $B_2H_4^{2-}$ plane, has a B-B distance of 1.629 Å and is 14.9 kcal mol^{-1} less stable. Clearly, the agreement between the theoretical and structural data for 1 is very good. Further calculations on the energy of the π-bonding and the rotation barrier in 1 are in progress.[16]

Acknowledgment. We thank the National Science Foundation and the donors of the Petroleum Research Fund, administered by the American Chemical Society, for financial support and Professors T. L. Allen, W. H. Fink, and R. Hoffmann for useful discussions. We also thank Professor A. Berndt for making data available to us prior to publication.

Registry No. 1, 139199-40-9; **2**, 139199-38-5.

Supplementary Material Available: Tables of data collection parameters, atom coordinates, bond distances, bond angles, anisotropic thermal parameters, and hydrogen coordinates (10 pages); listing of observed and calculated structure factors (17 pages). Ordering information is given on any current masthead page.

(14) Setzer, W. N.; Schleyer, P. v. R. *Adv. Organomet. Chem.* **1985**, *24*, 353.
(15) Kaufmann, E.; Schleyer, P. v. R. *Inorg. Chem.* **1988**, *27*, 3987.
(16) Allen, T. L.; Fink, W. H. Work in progress.

Three-Dimensional Microscopic ^1H NMR Imaging of Rigid Polymers

S. L. Dieckman,*,† P. Rizo,‡ N. Gopalsami,† J. P. Heeschen,§ and R. E. Botto∥

Materials and Components Technology Division and Chemistry Division, Argonne National Laboratory 9700 South Cass Avenue, Argonne, Illinois 60439 Laboratoire d'Electronique et de Technologie de l'Informatique, Dêpartment Systèmes C.E.A./C.E.N.G., 85X Avenue des Martyrs 38041 Grenoble Cedex, France The Dow Chemical Company Analytical Sciences Laboratory Midland, Michigan 48667

Received October 18, 1991

We report the first application of ^1H nuclear magnetic resonance (NMR) to obtain three-dimensional (3-D) spatially resolved images of a rigid polymer. The technique, which has been demonstrated on a polycarbonate sample, uses MREV-8 multiple-pulse homonuclear decoupling[1,2] in combination with 3-D back-projection.[3-6] The image provides a 3-D map of the proton content within the specimen to a spatial resolution of $150_x \times 150_y \times 150_z$ μm^3. The reconstructed surface-rendered image is a reasonably accurate reproduction of the specimen's complex topology.

The inherently broad line widths associated with homonuclear dipolar interactions of abundant proton spins in solids have hampered the rapid development of NMR imaging techniques for materials. Only within the last several years have effective imaging strategies been implemented to overcome broadening effects in rigid, protonated solids. Several techniques for proton NMR imaging of solids have been demonstrated,[6-15] but only in linear (1-D) or planar (2-D) fashion. Spatial discrimination in the third dimension has been difficult to achieve due to the inherently short proton transverse relaxation times (T_2s) in solids. This rapid decay of magnetization has precluded the use of spatial encoding methods, which are commonly used in liquids.[16,17]

Recent work in our laboratory has focused on the use of multiple-pulse coherent averaging of homonuclear broadened lines, which is applied in conjunction with back-projection techniques to obtain 3-D spatially encoded images of proton density. The

† Materials and Components Technology Division, Argonne National Laboratory.
‡ Laboratoire d-Electronique et de Technologie de l Informatique.
§ Dow Chemical Company.
∥ Chemistry Division, Argonne National Laboratory.

(1) Rhim, W.-K.; Elleman, D. D.; Vaughan, R. W. *J. Chem. Phys.* **1973**, *59*[7], 3740.
(2) Mansfield, P.; Grannell, P. K. *Phys. Rev. B* **1975**, *12*, 3618.
(3) Three-dimensional back-projection ^1H NMR imaging techniques were initially demonstrated and applied to the imaging of solutions.[4,5] More recently, the applicability of this technique to semi-solid materials has been demonstrated.[6]
(4) Lauterbur, P. C.; Lai, C.-M. *IEEE Trans.* **1980**, *27*, 1227.
(5) Lai, C.-M.; Lauterbur, P. C. *J. Phys. E* **1980**, *13*, 747.
(6) Dieckman, S. L.; Rizo, P.; Gopalsami, N.; Botto, R. E. *Proc. Mater. Res. Soc.* **1991**, *217*.
(7) Wind, R. A.; Yannoni, C. S. *J. Magn. Reson.* **1979**, *36*, 269.
(8) Garroway, A. N.; Baum, J.; Munowitz, M. G.; Pines, A. *J. Magn. Reson.* **1984**, *60*, 337.
(9) Chingas, G. C.; Miller, J. B.; Garroway, A. N. *J. Magn. Reson.* **1986**, *66*, 530.
(10) Cory, D. G.; Reichwein, A. M.; van Os, J. W. M.; Veeman, W. S. *Chem. Phys. Lett.* **1988**, *143*, 467.
(11) Miller, J. B.; Garroway, A. N. *J. Magn. Reson.* **1989**, *82*, 529.
(12) Ogura, Y.; Sekihara, K. *J. Magn. Reson.* **1989**, *83*, 177.
(13) Fry, C. G.; Lind, A. C.; Davis, M. F.; Duff, D. W.; Maciel, G. E. *J. Magn. Reson.* **1989**, *83*, 656.
(14) Rommel, E.; Hafner, S.; Kimmich, R. *J. Magn. Reson.* **1990**, *86*, 264.
(15) Sinton, S. W.; Iwamiya, J. H.; Ewing, B.; Drobny, G. P. *Spectroscopy* **1991**, *6*[3], 42.
(16) Miller, J. B. *Trends Analytical Chem.* **1991**, *10*[2], 59.
(17) Cory, D. G.; Veeman, W. S. *J. Magn. Reson.* **1989**, *84*, 392.

0002-7863/92/1514-2717$03.00/0

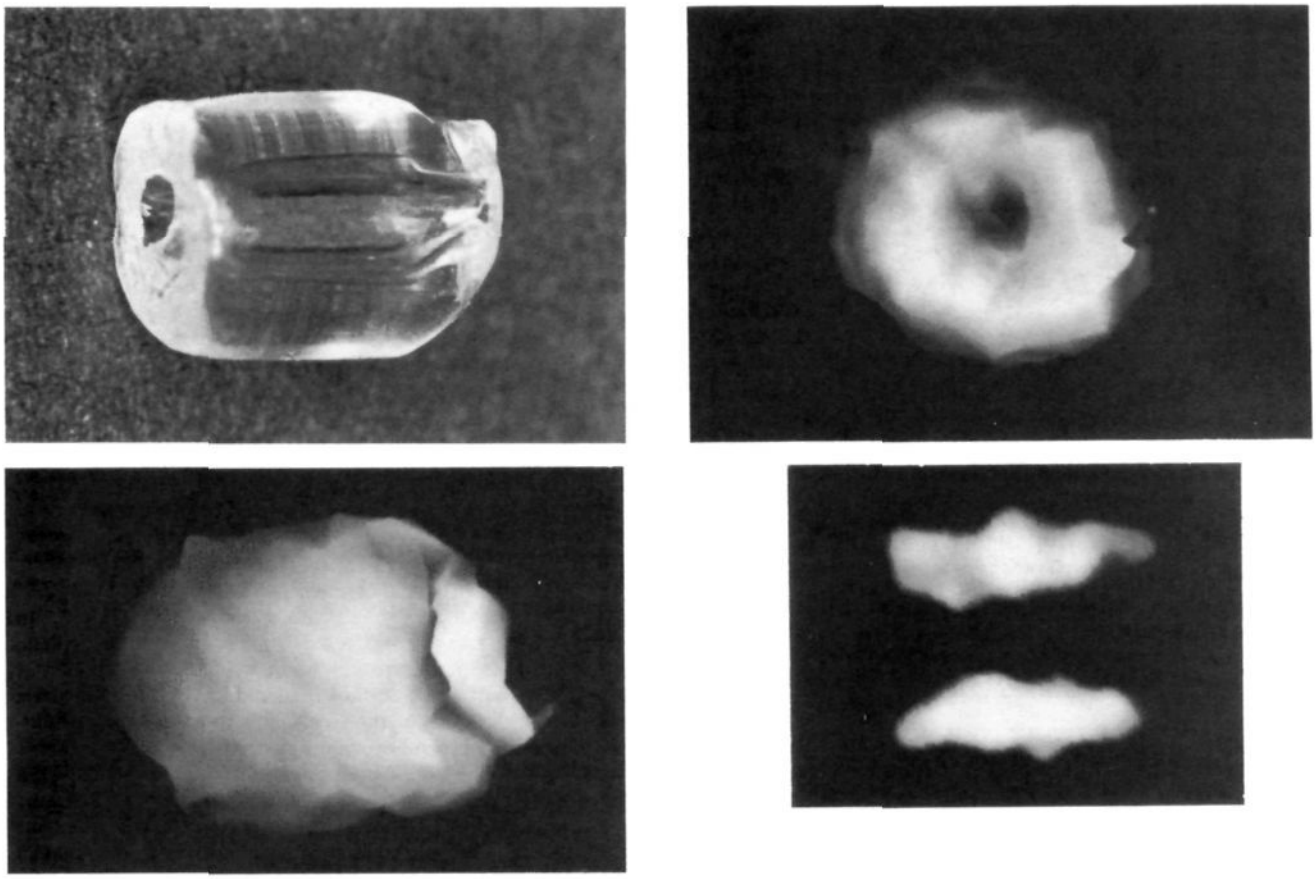

Figure 1. Optical photograph (A, top left), two orientations of the surface-reconstructed 3-D proton image (B and C, bottom left and top right), and a slice from the center of the 3-D image (D, bottom right) of an extruded polycarbonate specimen. 3-D NMR image data were obtained on a Bruker CXP-100 NMR spectrometer fitted with a home-built imaging accessory (described in detail elsewhere[20]). Data were collected with 128 data points acquired in nonquadrature mode by the MREV-8 pulse sequence. A 1.2-μs 90° pulse was achieved by approximately 200 W of rf with a 3.5-mm solenoidal coil. An interpulse delay time of 3.2 μs was used, giving a total cycle time of 38.4 μs. A total of 1600 projections (20 θ angles over $\pi/2$ radians × 80 ϕ angles over 2π radians) were acquired with a magnetic field gradient strength of 16 G/cm, and 64 averages were acquired per projection with a recycle delay time of 0.40 s. Data acquisition with these parameters required 12 h. Data were reconstructed on a local Vax-8700 with software written in-house. The final 3-D image was reconstructed with a 3-D Radon inversion code developed at LETI. The 3-D surface-rendered images were rendered, displayed, and photographed from an Ardent/Titan workstation by a commerical image-production package titled Application Visualization System (available from Stardent Computer, Inc.). The slice was additionally processed using a planar 4 × 4 median filter. Final resolution was $150_x \times 150_y \times 150_z$ μm^3.

MREV-8 pulse sequence has been applied in the presence of a strong magnetic field gradient (MFG) to generate frequency-encoded 1-D projections of the object space parallel to the MFG vector. A series of projections was acquired by electronically rotating the MFG vector in classical spherical coordinate space about the sample.[6] The images were subsequently calculated from the series of 1-D phased projections using 3-D Radon transform inversion that was implemented as proposed by Grangeat et al.[18]

An optically transparent, extruded BPA polycarbonate (bisphenol A polycarbonate, Calibre[19]) sample with unusual topology was chosen for examination (see Figure 1A). The specimen had a distorted cylindrical geometry (3 mm long × 2 mm in diameter) and contained a hole, which had formed during extrusion, along the main axis. The hole measured 400 and 150 μm in diameter at its entrances and was slightly larger in diameter in the specimen's interior.

The MREV-8 sequence narrows the polycarbonate proton line width of the static specimen from 35 to 0.85 kHz. The remaining static line width results from a combination of magnetic susceptibility effects, chemical shift anisotropy, residual dipolar broadening, and distribution of isotropic chemical shifts. However, it is known that the frequency offset response of the MREV-8 sequence reduces decoupling efficiency as the difference between the decoupling frequency and the observed chemical shift becomes larger. This reduction generates a nonlinear response in amplitude and in observed chemical shift as a function of decoupling frequency. In imaging, where linearity is often required for accurate image reconstruction, these nonlinearities can cause severe artifacts. In an attempt to minimize these effects on image quality, images were acquired by using a moderate MFG strength to limit changes in line widths from 0.85 to 2.0 kHz (chemical shift scaling factor of 2.12 to 2.71) across the 1-D projections.

Two orientations of the surface-rendered 3-D proton image of the polycarbonate specimen are presented in Figure 1B,C. A slice taken from a single plane in the center of the specimen is also presented in Figure 1D. The major topological features are accurately reproduced in the image, which has a spatial resolution of $150_x \times 150_y \times 150_z$ μm^3. The hole is clearly visible in Figure 1C,D, in particular the constriction toward the posterior end of the image. Discontinuous features on the surface represent image artifacts primarily caused by resonance offset effects as discussed above, and to a lesser extent, by 3-D surface-tiling errors caused by poor signal-to-noise ratio. Application of more robust multiple-pulse sequences, such as the 48-pulse sequence,[21] may provide

(18) Grangeat, P.; Hatchadourian, G.; Le Masson, P.; Sire, P. *Logiciel Radon, Notice Descriptive des Algorithmes et des Programmes*, Version 2.1 du 13-04-1990, LETI/DSYS/SETI/90-180 PS, Grenoble, France, le 11 Mai, 1990.

(19) Calibre is a registered trademark of The Dow Chemical Company.

(20) Gopalsami, N.; Foster, G. A.; Dieckman, S. L.; Ellingson, W. A.; Botto, R. E. *Development of NMR Imaging Probes for Advanced Ceramics*; Rev. Prog. in QNDE; Thompson, D. O., Climenti, D. E., Eds.; Plenum Press: 1990.

(21) Cory, D. G.; Miller, J. B.; Garroway, A. N. *J. Magn. Reson.* **1990**, *90*, 205.

more efficient line narrowing that leads to higher image resolution and less severe artifacts. Also, development of postprocessing techniques to correct for resonance offset effects is currently underway.

In addition to 3-D mapping of proton density, an immediate extension of this technique is the examination of polymer microstructure (such as cross-link density, homogeneity in blends, and crystallinity) utilizing relaxation[22] (T_1 and $T_{1\rho}$) and spin-diffusion-weighted image protocols. Direct experimental measurement of morphological changes affected by stress, physical aging, phase transitions, annealing, mechanical and thermal degradation, and oxidation is also possible.

Acknowledgment. We are pleased to acknowledge that the financial support for this work was provided by the U. S. Department of Energy through the Assistant Secretary for Conservation and Renewable Energy, Office of Transportation Systems, Advanced Materials Development Program; the Assistant Secretary for Fossil Energy, Advanced Research and Technology Development, Materials Research Program; and the Office of Basic Energy Sciences, Division of Chemical Sciences, under Contract W-31-109-Eng-38.

(22) Dieckman, S. L.; Gopalsami, N.; Botto, R. E. *Energy Fuels* **1990**, *4*[4], 417.

Ab Initio Calculations of the Relative Energies of Homocub-1(9)-ene and Homocub-9-ylidene. How Strong Is the Twisted "π" Bond in the Olefin? What Is the Ground State of the Carbene?

David A. Hrovat and Weston Thatcher Borden*

Department of Chemistry
University of Washington
Seattle, Washington 98195
Received December 13, 1991

Rearrangements of carbenes to olefins are usually highly exothermic and, hence, irreversible reactions.[1] Nevertheless, bridgehead olefins with sufficient torsional strain are capable of undergoing reversion to carbenes.[2] The best and most recently studied example of the latter process was discovered by Eaton and Hoffmann in the rearrangement of 9-phenylhomocub-1(9)-ene (**1a**) to 1-phenylhomocub-9-ylidene (**2a**).[3] Subsequent investigations in the desphenyl series demonstrated that the olefin (**1b**) can also be formed from the carbene (**2b**),[4] and experiments by Jones, Platz, and co-workers have found the equilibrium constant for this reaction to be approximately unity at room temperature.[5]

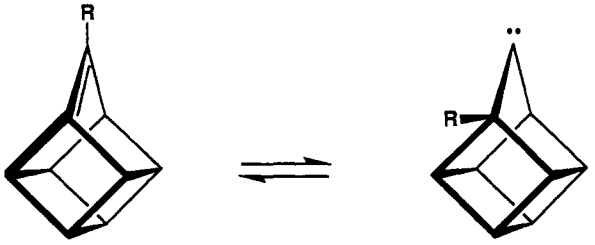

1a, R = Ph
1b, R = H

2a, R = Ph
2b, R = H

(1) Kirmse, W. *Carbene Chemistry*, 2nd ed.; Academic Press: New York, 1971. Jones, M., Jr., Moss, R. A., Eds. *Carbenes*; Wiley: New York, 1973 (Vol. 1), 1975 (Vol. 2).

(2) Chan, T. H.; Massuda, D. J. *J. Am. Chem. Soc.* **1977**, *99*, 936. Barton, T. J.; Yeh, M.-H.; Baird, M. S. *Tetrahedron Lett.* **1987**, *28*, 6421.

(3) Eaton, P. E.; Hoffmann, K.-L. *J. Am. Chem. Soc.* **1987**, *109*, 5285. The rearrangement was subsequently shown to involve shift of a C–C bond of the homocubyl skeleton, rather than phenyl migration. Eaton, P. E.; White, A. J. *J. Org. Chem.* **1990**, *55*, 1321.

(4) (a) Jones, M., Jr.; Chen, N. *J. Phys. Org. Chem.* **1988**, *1*, 305. Chen, N.; Jones, M., Jr. *Tetrahedron Lett.* **1989**, *30*, 4055. (b) Eaton, P. E.; Appel, R. B. *J. Am. Chem. Soc.* **1990**, *112*, 4055.

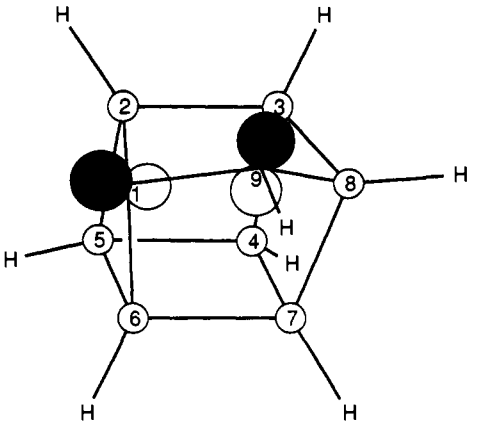

Figure 1. GVB/6-31G* optimized geometry for **1b**, depicting the alignment of the atomic orbitals at C_1 and C_9 that results from the pyramidalization at C_9.

Table I. Relative Energies Calculated at the GVB/6-31G* Level for Singlets and at the ROHF/6-31G* Level for Triplets

molecule, state, geometry, symmetry	energy (kcal/mol)
1b, singlet, equilibrium geometry, C_1	3.8
1b, singlet, C_9 planar, C_s	8.2
1b, triplet, equilibrium geometry, C_1[a]	5.0
2b, singlet, equilibrium geometry, C_s[b]	0[c]
2b, triplet, equilibrium geometry, C_{2v}	1.6

[a] This geometry, with the hydrogen at C_9 31.8° out of the plane defined by C_1, C_8, and C_9, is lower by 1.4 kcal/mol than the optimized C_s geometry in which the hydrogen at C_9 lies in this plane. [b] This geometry, in which C_9 is tilted 13.0° out of the plane defined by C_1, C_5, C_4, and C_8, is 0.2 kcal/mol lower in energy than the optimized C_{2v} structure, in which all five carbons lie in the same plane. [c] E = −345.2291 hartrees.

In this communication we report the results of ab initio calculations on the relative energies of **1b** and **2b**. Our calculations not only confirm that **1b** and **2b** are nearly isoenergetic but also they predict that only 4.4 kcal/mol is required to break the highly twisted "π" bond in olefin **1b**, and they indicate a singlet ground state for carbene **2b**.

GVB calculations that correlate one pair of electrons provide adequate wave functions for the weakly bonding pair of electrons in a deformed alkene[6] and also for the pair of nonbonding electrons in a singlet carbene.[7] Therefore the geometries of both **1b** and **2b** were optimized[8] with GVB-PP(1) calculations,[9] using both the 3-21G[10] and 6-31G* basis sets.[11] Vibrational analyses,[12] per-

(5) Chen, N.; Jones, M., Jr.; White, W. R.; Platz, M. *J. Am. Chem. Soc.* **1991**, *113*, 4981.

(6) See, for example: (a) Salem, L.; Rowland, C. *Angew. Chem., Int. Ed. Engl.* **1972**, *11*, 92. (b) Borden, W. T. In *Diradicals*; Borden, W. T., Ed.; Wiley: New York, 1982; pp 1–72.

(7) Reviews: (a) Davidson, E. R. In *Diradicals*; Borden, W. T., Ed.; Wiley: New York, 1982; pp 73–105. (b) Shavitt, I. *Tetrahedron* **1985**, *41*, 1531. For a more recent computational study of methylene, see: Carter, E. A.; Goddard, W. A., III. *J. Chem. Phys.* **1987**, *86*, 862.

(8) Optimized geometries are available as supplementary material. Ordering information is given on any current masthead page.

(9) Geometries were optimized with Gaussian 90: Frisch, M. J.; Head-Gordon, M.; Trucks, G. W.; Foresman, J. B.; Schlegel, H. B.; Raghavachari, K.; Robb, M. A.; Binkley, J. S.; Gonzalez, C.; Defrees, D. J.; Fox, D. J.; Whiteside, R. A.; Seeger, R.; Melius, C. F.; Baker, J.; Martin, R. L.; Kahn, L. R.; Stewart, J. J. P.; Topiol, S.; Pople, J. A. Gaussian, Inc., Pittsburgh, PA, 1990.

(10) Binkley, J. S.; Pople, J. A.; Hehre, W. J. *J. Am. Chem. Soc.* **1980**, *102*, 939.

(11) Hariharan, P. C.; Pople, J. A. *Theor. Chim. Acta* **1973**, *28*, 213.

(12) Vibrational analyses were performed with analytical second derivatives, using GAMESS: Dupuis, M.; Spangler, D.; Wedolowski, J. J. Modified by Schmidt et al.: Schmidt, M. W.; Baldridge, K. K.; Boatz, J. A.; Jensen, J. H.; Koseki, S.; Gordon, M. S.; Nguyen, K. A.; Windus, T. L.; Elbert, S. T. *QCPE Bull.* **1990**, *10*, 52.

0002-7863/92/1514-2719$03.00/0